



<b>Publication Year</b>	2018
<b>Acceptance in OA @INAF</b>	2020-09-28T09:51:33Z
<b>Title</b>	A global optimisation study of the low-lying isomers of the alumina octomer (Al <sub>2</sub> O <sub>3</sub> ) <sub>8</sub>
<b>Authors</b>	Gobrecht, David; Decin, Leen; CRISTALLO, Sergio; Bromley, Stefan T.
<b>DOI</b>	10.1016/j.cplett.2018.09.018
<b>Handle</b>	<a href="http://hdl.handle.net/20.500.12386/27488">http://hdl.handle.net/20.500.12386/27488</a>
<b>Journal</b>	CHEMICAL PHYSICS LETTERS
<b>Number</b>	711

# A global optimisation study of the low-lying isomers of the alumina octomer $(\text{Al}_2\text{O}_3)_8$

David Gobrecht<sup>✉a</sup>, Leen Decin<sup>a</sup>, Sergio Cristallo<sup>b,c</sup>, Stefan T. Bromley<sup>d,e</sup>

<sup>a</sup>*Instituut voor Sterrenkunde, KU Leuven, Celestijnenlaan 200D, B-3001 Leuven, Belgium*

<sup>b</sup>*INAF - Osservatorio Astronomico d'Abruzzo, Via mentore maggini s.n.c., I-64100 Teramo, Italy*

<sup>c</sup>*INFN - Sezione di Perugia, via A. Pascoli, I-06123, Perugia, Italy*

<sup>d</sup>*Departament de Ciència de Materials i Química Física & Institut de Química Teòrica i Computacional (IQTCUB), Universitat de Barcelona, E-08028 Barcelona, Spain*

<sup>e</sup>*Institució Catalana de Recerca i Estudis Avançats (ICREA), E-08010 Barcelona, Spain*

---

## Abstract

We employ the Monte-Carlo Basin-Hopping (MC-BH) global optimisation technique with inter-atomic pair potentials to generate low-energy candidates of stoichiometric alumina octomers  $((\text{Al}_2\text{O}_3)_8)$ . The candidate structures are subsequently refined with density functional theory calculations employing hybrid functionals (B3LYP and PBE0) and a large basis set (6-311+G(d)) including a vibrational analysis. We report the discovery of a set of energetically low-lying alumina octomer clusters, including a new global minimum candidate, with shapes that are elongated rather than spherical. We find a stability limit for these and smaller-sized clusters at a temperature of  $T \simeq 1300 - 1450$  K corresponding to a phase transition in liquid alumina.

*Keywords:* aluminum oxide, molecular clusters, global optimisation, nucleation

---

## 1. Introduction

Alumina clusters play a role in atmospheric chemistry [1]. Being artificially produced by rocket flights,  $\text{Al}_2\text{O}_3$  cluster aerosols impact the Earth's atmospheric chemistry as they act as catalysts. Moreover, owing to their high thermal stabilities and (near)-infrared properties, alumina clusters are promising candidates to form the seed nuclei of dust formation in oxygen-rich AGB stars [2, 3, 4, 5]. Although silicate dust constitutes the major part of oxygen-rich cosmic dust, its nucleation solely from gas-phase precursors is energetically hampered and explicitly ruled out for SiO [6, 7] and MgO [8, 9]. Instead, it is more likely that the silicate dust forms on top of pre-existing seed nuclei. These seed nuclei must form from available atoms and molecules, and have to sustain the extreme thermodynamic conditions close to the stellar surface. In oxygen-dominated regimes, the latter requirements are fulfilled by highly refractory metal oxides such as alumina ( $\text{Al}_2\text{O}_3$ ) and titania ( $\text{TiO}_2$ ). Studies on stardust grains from pristine meteorites show

---

<sup>✉</sup>corresponding author

*Email address:* david.gobrecht@kuleuven.be (David Gobrecht<sup>✉</sup>)

*Preprint submitted to Chemical Physics Letters*

October 5, 2018

larger sizes and greater amounts of alumina, compared with titania [10, 11]. Thus, we presume that it is most likely that alumina initiates stardust synthesis in oxygen-rich conditions.

Apart from a pure scientific interest alumina clusters are also of practical use. Owing to their large refractories, high hardness, high stabilities, high insulation capabilities, and optical transparency [12] alumina clusters serve as components for diverse purposes and applications. Over the past few decades, nano-sized alumina fibers have been synthesized by diverse techniques (hydrothermal or solvothermal, sol-gel techniques, electrospinning, extrusion, chemical vapor deposition) [13] and have attracted a lot of attention. The fibers are used in electronics, informatics, and communications [14]. Moreover, owing to its bio-compatibility, alumina nanofibers are also used for drug delivery. In the laboratory, clusters of nano-sized alumina can be produced in deionized water by laser ablation of aluminum targets [15].

There are several bulk polymorphs for alumina. The most stable polymorph at standard conditions ( $p = 1$  atm,  $T = 298$  K) is the hexagonally, closed-packed  $\alpha$ -alumina which is the main component of corundum [16]. Other alumina polymorphs are  $\beta$ ,  $\gamma$ ,  $\delta$ ,  $\eta$  and  $\chi$ -alumina that represent the most stable alumina bulk forms at elevated temperatures. All these crystalline bulk forms have trivalent  $\text{Al}^{3+}$  cations and divalent  $\text{O}^{2-}$  in common. In this work, we compare the properties of our individual clusters with respect to each other, and with  $\alpha$  alumina. Previous studies have shown that alumina clusters substantially deviate from the bulk-like analogs [17, 18]. In the size regime with dimension  $d \leq 1$  nm (which corresponds to the size range from the monomer to the octomer,  $n=8$ ), diverse geometries (flat, cage-like, compact) represent the most stable isomer structures [19, 20, 21]. The alumina octomer corresponds to the first cluster size at which we find differences with previously reported candidate global minima in the literature. We revisit also smaller cluster sizes ( $n < 8$ ) and we find the same structural isomers as found in the thorough study by [20]. As a result of strong (attractive and repulsive) Coulomb forces between O-anions and Al-cations, all favourable clusters have a strictly alternating cation-anion ordering in common.

This letter is organized as follows. In Section 2, we describe the methods to find low-energy alumina octomer structures and their subsequent refinement at the DFT (Density Functional Theory) level. The results of our calculations are presented in Section 3. Finally, we discuss and summarize our new findings in Section 4.

## 2. Methods

### 2.1. Global optimisation searches

An alumina octomer, i.e.  $(\text{Al}_2\text{O}_3)_8$ , has 40 atoms and a total of  $3 \times 40 = 120$  degrees of freedom resulting in a huge configurational space. A complete exploration of this space would require enormous amount of computational power and is beyond the current computing ability. To reduce the number of possible structural configurations to explore (and hence also the computational effort) a global optimisation search for low-energy octomer isomers is performed. We employ the Monte-Carlo Basin-Hopping (MC-BH) global optimisation technique [22] with inter-atomic pair potentials of an Al-O system to find candidate structures. For our purposes, we use an in-house, modified version of the GMIN programme [23]. The general form of the inter-atomic Buckingham pair potential (including the Coulomb potential) reads:

Table 1: The parameter ranges used in this study to compute the inter-atomic Buckingham pair potential. Charges  $q(\text{Al})$  and  $q(\text{O})$  are given in atomic units,  $A$  in eV,  $B$  in  $\text{\AA}$   $C$  in  $\text{eV \AA}^{-6}$ .

$q(\text{Al})$	$q(\text{O})$	A(Al-O)	B(Al-O)	C(Al-O)	A(O-O)	B(O-O)	C(O-O)
+3, +2.4	-2, -1.6	2409.5	0.2649	0.0	22764.0	0.14	27.88
+3, +2.4	-2, -1.6	4534.2	0.2649	0.0	25.410	0.6937	32.32

$$U(r_{ij}) = \frac{q_i q_j}{r} + A \exp\left(-\frac{r_{ij}}{B}\right) - \frac{C}{r_{ij}^6} \quad (1)$$

where  $r_{ij}$  is the relative distance of two atoms,  $q_i$  and  $q_j$  the charges of atom  $i$  and  $j$ , respectively, and  $A$ ,  $B$  and  $C$  the Buckingham pair parameters. The first term in equation 1 represents the Coulomb law, the second term the short-range, steric repulsion term accounting for the Pauli principle, and the last term describes the attractive van-der-Waals interaction. The potential describes the repulsion and attraction of charged particles, in this case, of aluminum and oxygen ions within a  $(\text{Al}_2\text{O}_3)_8$  cluster. As lightest members of group III and group VI elements in the periodic table, Al and O form ionic bonds. The strong difference in electro-negativity,  $\Delta \text{EN}=2.03$ , strongly suppresses the presence of covalent bonds. To reduce the probability to miss stable configurations in our searches we perform test calculations by swapping Al and O atoms of the most stable configurations. These tests account for atomic segregation (i.e. covalent bonds between identical atoms). The steric repulsion term is motivated by the fact that atoms are not dot-like but occupy a certain volume in space. We use the simplified form of the Buckingham pair potential and omit the repulsive  $r^{-12}$  Lennard-Jones term. Effectively, the latter term acts only on very short distances which is already taken into account by values of the parameters  $A$  and  $B$ . In the present approach we approximately account for the polarization effects by reducing the formal charges of the Al-cations and the O-anions by 10-20%.

We apply two different parameter sets that are listed in Table 1. The first listed set (set 1) is commonly used for structure optimisation of Al-O systems (see e.g. [21]). The second parameter set in the last line of Table 1 corresponds to  $\text{Ag}^{+3}\text{-O}^{-2}$  parameters published by [24]. With exception of the value of  $A(\text{Ag-O})$ , the other parameters are identical to the shell  $\text{Al}^{3+}\text{O}^{2-}$  set of [25]. Set 2 complements set 1 in the sense that it covers a different parameter space accounting for structural families that could not (or hardly) be found with set 1. For example, set 1 tends to result in compact geometries, but structural families like void cages and open-cage-like clusters are underrepresented. Both parameter sets are explored with a variety of different seed structures (i.e. initial geometries).

In summary, we use two different parameter sets, dozens of seed structures and different temperatures ( $T = 300\text{-}3000$  K) in order to cover an extensive number of structural possibilities. Although the use of force fields is an approximation, their use enables us to perform tractable thorough searches. With our force-field approach we hope to have minimized the probability to miss a stable alumina octomer.

## 2.2. Optimisation at the DFT level

Once multiple sets of candidate structures with different seed geometries, temperatures and parameter sets are found, we refine the  $\sim 100$  most favourable candidate structures with hybrid density functional theory (DFT) methods. We use two different density functionals, B3LYP [26] and PBE0 [27], in combination with the 6-311+G(d) basis set and perform the calculations with the help of the computational chemistry software package Gaussian09 [28]. The DFT calculations are performed at 0 K and 0 atm. In the Born-Oppenheimer approximation used here the Potential Energy Surface (PES) does not depend on temperature. Hence, the optimised cluster geometry is also temperature-independent. However, the vibrational population and the computation of the thermodynamic quantities (enthalpy, entropy, Gibbs free energy) depend on temperature. The thermal corrections are evaluated at standard conditions for temperature and pressure ( $T = 298.15$  K,  $p = 1$  atm). We include a vibrational analysis to calculate appropriate partition functions for any other conditions and to exclude possible transition states.

## 3. Results

### 3.1. Minima structures

Our lowest energy candidate global minimum octomer ( $\text{Al}_2\text{O}_3$ )<sub>8</sub> structure (hereafter **8A**) calculated at the B3LYP/6-311+G(d) level of theory is displayed in Figure 1. The structure has a rotational symmetry and belongs to the  $C_2$  point symmetry group. Its potential energy is lower by 0.15 eV relative to the next higher-lying isomer. With the PBE0/6-311+G(d,p) functional/basis set **8A** represents the second lowest-energy structure (relative energy difference of 0.17 eV with respect to **8B** - see below) that we find. The HOMO-LUMO gap in the B3LYP (PBE0)- optimised new structure is 4.93 (5.45) eV.

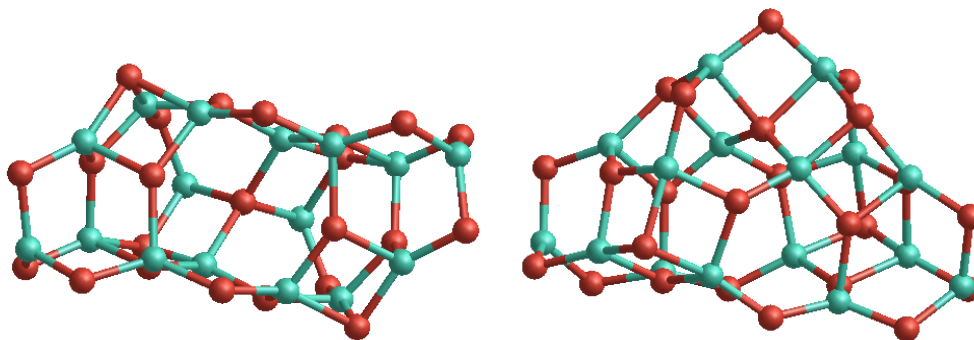


Figure 1: The global minimum structure **8A** at the B3LYP/6-311+G(d) level seen from two distinct perspectives (that are perpendicular to each other). Al atoms are in green, O atoms in red.

Our search also resulted in the discovery of another alumina octomer cluster (hereafter **8B**) that is displayed in Figure 2. **8B** shows a  $C_s$ -symmetric structure. However, during the optimisation at the DFT level, the symmetry of **8B** is distorted and the assigned point symmetry group for **8B** is  $C_1$ . Structure **8B** is the lowest-energy configuration

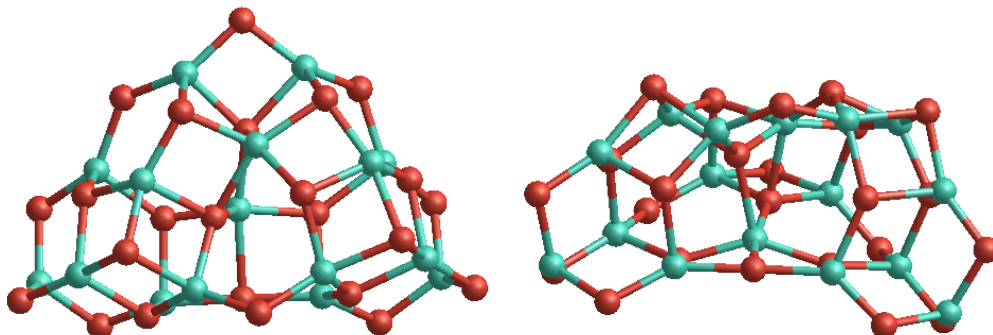


Figure 2: The global minimum structure **8B** at the PBE0/6-311+G(d) level seen from two distinct perspectives.

that we find with the PBE0 functional and the second-lowest (relative energy 0.15 eV) with the B3LYP functional. The HOMO-LUMO gap in the B3LYP (PBE0)-optimized structure **8B** is 4.67 (3.60) eV which is less than for **8A**.

Further energetically low-lying alumina octamer isomers that have been found in this study are shown in Figure 3. All of the latter local minima structures are not symmetric and belong to the  $C_1$  point group. Structure **8C** has relative potential energy 0.35 eV (0.25 eV) above the minimum with the B3LYP (PBE0) functional.

**8D**, **8E** and **8F** are located 0.97 (1.14), 0.98 (0.71) and 1.43 (1.24) eV above the global minimum structure **8A** (**8B**), respectively. In particular, we note that **8D** and **8E** are almost degenerate at the B3LYP level of theory, but have a significant difference (0.43 eV) as calculated with the PBE0 functional. All structures - except **8F**, but including **8A** and **8B** - exhibit an overall elongated geometry where one dimension ( $\sim 9-10$  Å) is significantly longer than the other two dimensions (typically  $\sim 6-7$  Å). This may suggest an inherent tendency for a deviation from sphericity in a homogeneous nucleation scenario for alumina.

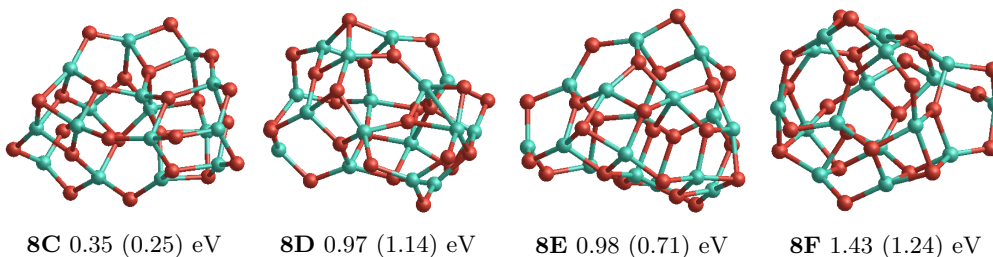


Figure 3: Energetically low-lying alumina octamer structures with energetic ordering according to DFT optimisations using the B3LYP functional.

In Figure 4, the predicted global minimum structure in ref. [19] (hereafter **8G**) is shown. **8G** has two mirror planes, two rotational symmetries and belongs to the  $D_{2d}$  space group. **8G** has a potential energy 1.56 (0.88) eV above the minima structures **8A** (**8B**).

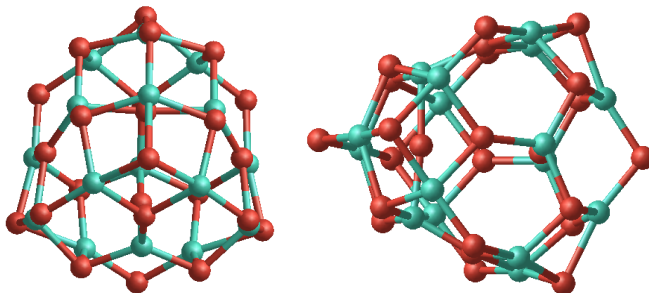


Figure 4: The minimum structure **8G** seen from two distinct perspectives.

Five other low-lying alumina octomer isomers were predicted in ref. [21], see Figure 7 in their paper) using a gradient-based genetic algorithm (GA-LBFGS) and a Buckingham pair potential. We have also found the latter five isomers and investigated them on the DFT level of theory. Structures A, B, D and E in ref. [21] relax to structure **8G** during a DFT optimisation with the hybrid functionals B3LYP and PBE0 and thus do not represent truly distinct structural isomers. The investigation of structures C and E in Figure 7 in ref. [21] at a DFT level results in the same isomer (see Figure 5) with a relative energy 2.77 (1.89) eV above 8A (8B). It has a mirror plane and space group  $C_{2v}$ .

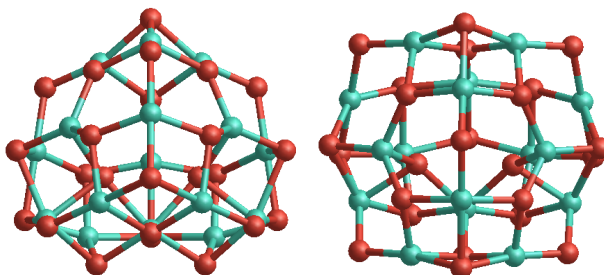


Figure 5: The stable structure **8H** seen from two distinct perspectives.

Recently, the structural family of  $(Al_2O_3)_n$  hollow spheres and bubble clusters has been studied for certain sizes ( $n=10, 12, 16, 18, 24$  and  $33$ ) [29]. The latter structures are characterized by Al-atoms with coordination number 3 and O-atoms that are 2-coordinated. For  $n=8$ , we also find a member of the hollow spheres, or “bubble” family (see Figure 6). Cluster 8I has a very symmetric peanut-shaped geometry and belongs to the  $D_{2h}$  point group. It has an electronic energy 5.31 (7.67) eV above the global minimum. We report the finding of six new isomer structures (8A, 8B, 8C, 8D, 8E, 8F). The previously reported structures 8G, 8H and 8I have potential energies that are significantly higher than 8A-8F.

### 3.2. Rotational constants

The rotational constants of the two isomers 8A and 8B are tabulated in Table 2. The rotational constants obtained with the PBE0 functional are marginally larger ( $\sim 1\%$ )

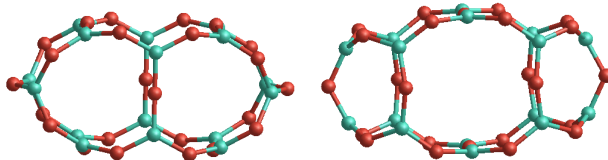


Figure 6: The stable structure **8I**

Table 2: Rotational constants for 8A and 8B in (GHz)

Rot. Constants GHz	8A		8B	
	(B3LYP)	PBE0	B3LYP	PBE0
$B_x$	0.113953	0.115163	0.090181	0.091319
$B_y$	0.062404	0.063075	0.084215	0.085045
$B_z$	0.056707	0.057285	0.084212	0.085042

that those obtained with the B3LYP functional. This is a consequence of the slightly more compact geometry of the PBE0 optimized structures leading to lower moments of inertia and higher rotational constants. Owing to its  $C_2$  symmetry 8B has two almost identical constants ( $B_y$  and  $B_z$ ).

### 3.3. Bond distances, coordination and charges

The Al-O bond distances of the clusters 8A, 8B, and 8G, and of the crystalline bulk ( $\alpha$ -alumina) are shown in Figure 7. Al-Al and O-O bonds do not appear owing to the strong Coulomb repulsion of ions with the same (or similar) charge. The Al-O bond lengths of the clusters 8A, 8B, and 8G, as well as of  $\alpha$ -alumina form two populations, at short and at long bond lengths. The short bond peaks at 1.74 Å, and the long bond at 1.845 for structure 8A, for 8B the peaks are located at 1.745 Å and 1.855 Å, whereas they lie around 1.765 Å and 1.850 Å for 8G. Also in the bulk phase,  $\alpha$  alumina exhibits Al-O bonds with two different lengths being located at 1.972 Å and at 1.855 Å.

It is apparent that the clusters and the bulk exhibit bond lengths of around 1.85 Å. However, the most prominent feature of  $\alpha$ -alumina located at 1.972 Å is largely absent in the clusters and vice versa, inter-atomic distances smaller than 1.8 Å do not appear in  $\alpha$ -alumina, but account for a significant fraction of the cluster bonds. In 8A, 14 out of 16 Al cations are 4-coordinated, the remaining 2 Al are 3-coordinated, whereas 11 oxygen anions are 2-coordinated, 12 O atoms 3-coordinated and just one 4-coordinated. We count 62 Al-O bonds in total. The situation is similar for isomer 8B: It has 12 4-coordinated, 2 3-coordinated and 2 5-coordinated Al cations, respectively. The oxygen anions are 2-coordinated (10), 3-coordinated (12) and 4-coordinated (2). A total of 64 Al-O bonds is present in 8B. Contrary, structure 8G exhibits 12 4-coordinated, 4 5-coordinated, but no 3-coordinated Al cations. Also in the oxygen coordination 8G differs from 8A and 8B: 16 O anions are 3-coordinated, 6 O ions are 2-coordinated and 2 O ions are 4-coordinated, respectively. The number of Al-O bonds is 68 and thus slightly higher than in 8A and 8B. In  $\alpha$ -alumina, Al cations are 6-coordinated and O anion 4-coordinated. The average coordination in the crystalline bulk is (as expected) higher than for the clusters. In the clusters, a considerable fraction of the atoms are located

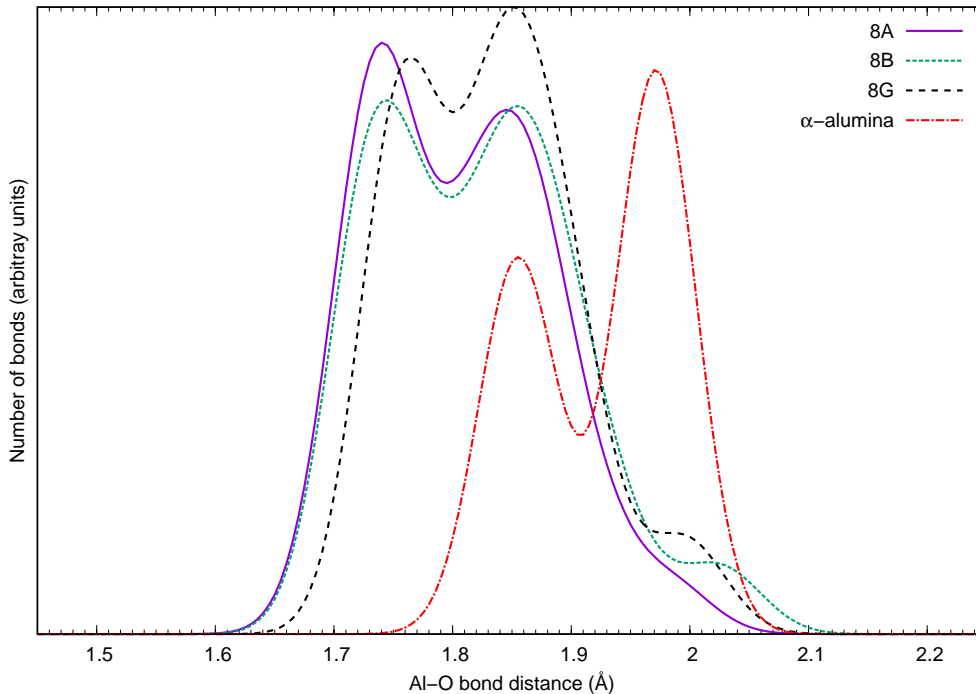


Figure 7: The Al-O bond lengths of 8A, 8B, 8G and  $\alpha$ -alumina. The curves are fitted with a Gaussian distribution and a half width  $\gamma=0.03\text{\AA}$ .

Table 3: Mulliken charge analysis for isomers 8A, 8B, 8G and  $\alpha$ -alumina (in atomic units)

charge	8A	8B	8G	8I	$\alpha$ -alumina
$q(\overline{Al})$	0.42 (0.30)	0.34 (0.24)	0.22 (0.09)	0.46 (0.36)	1.38 [30]
$q(\overline{O})$	-0.28 (-0.20)	-0.23 (-0.16)	-0.15 (-0.06)	-0.31 (-0.23)	-0.92(= $2/3 \times 1.38$ )

on the surface. Consequently, part of their atomic "neighbors" are missing and their coordination is lower.

In Table 3, the Mulliken charges of the presented clusters are shown. We also include a value for the average charge of  $\alpha$ -alumina in the bulk phase ( $q(\overline{Al})=+1.38$  e, [30]). However, we note that formal charge calculations strongly depend on the used basis set and functional and a comparison to the clusters is biased. In general, we find that the most stable isomers have higher formal atomic charges than the energetically less favourable clusters. Cluster 8I represents an exception, as it exhibits the largest average charges of all investigated clusters, but represents one of the energetically least stable ones due to its comparatively low coordination.

### 3.4. Bond angles

In Figure 8, the Al-O-Al and O-Al-O bond angles are displayed for structures 8A, 8B, 8G and  $\alpha$ -alumina. The latter exhibits characteristic angles at  $79.6^\circ$ ,  $84.6^\circ$ ,  $86.4^\circ$ ,  $90.8^\circ$ ,

93.6° and 132.2° and 164.2° degrees. The isomers 8A and 8B show a broad distribution of bond angles in the range between 80 and 180 degrees. Compared with 8G, and the crystalline phase ( $\alpha$ -alumina) the angle distribution of 8A and 8B is broader and has less pronounced peaks. The latter can be explained by the higher degree of symmetry in structure 8G, since owing to its internal plane symmetry, every angle appears twice. The crystalline form of alumina shows the fewest and most pronounced peaks, owing to symmetry reasons.

The difference of the bulk to the clusters can be explained by the finite-size geometries of the clusters. Whereas in  $\alpha$ -alumina the periodicity of the crystal implies a homogeneous spatial occupation by the Al and O atoms, the clusters are largely empty in their interiors and the atoms reside on the surface. As a consequence the cluster bond angles are systematically larger than in  $\alpha$ -alumina.

### 3.5. Vibrational analysis

An alumina octomer has 40 atoms, consequently the number of vibrational degrees of freedom (i.e. vibration modes) is  $3 \times 40 - 6 = 114$ . The vibrational infrared (IR) spectra of 8A, 8B, and 8G are shown as a function of wavelength in Figure 9. We use a Lorentzian function to describe the distribution of the peaks with a half-width at half-maximum  $\gamma = 0.2$ .

The majority of the IR modes of all shown clusters are located in a wavelength range between 10 and 20  $\mu\text{m}$  with a culmination point at 10-11  $\mu\text{m}$ . For structure 8A, the most intense vibration modes are located at wavelengths 10.012 (9.894), 10.985 (10.828), 10.729 (10.587) and 11.064 (10.921)  $\mu\text{m}$  for the B3LYP (PBE0) functional, respectively. For cluster 8B, the 10.348 (10.253), 10.126 (10.005), 11.009 (10.871) and 11.473 (11.329)  $\mu\text{m}$  for the B3LYP (PBE0) functional, respectively. These latter dominating vibrations are attributed to Al-O stretching and bending modes. A complete table with all vibrational frequencies for 8A and 8B can be found in the Appendix.

We investigate isomers 8A, 8B, and 8G also with the SDD (Stuttgart/Dresden) basis set including a vibrational analysis in order to benchmark with the results of ref. [19] who predicted isomer 8G as the global minimum. However, we found that vibrational calculations employing the SDD basis set led to imaginary frequencies for 8A, 8B, 8G which do not appear using a larger basis set (6-311+G(p)). We conclude that the SDD basis set is not adequate to describe alumina clusters and that all vibrational frequencies are real. Hence, clusters 8A, 8B, and 8G correspond to real minimum structures (and not transition states).

The differences in the IR spectra between PBE0- and B3LYP-based calculations are small and the tiny relative shifts in wavelengths arise - among other reasons - due to the slightly shorter bond distances obtained with the PBE0 functional, compared to the B3LYP functional (as for the rotational constants).

The vibrational zero-point energies of isomers 8A, 8B, and 8G are given in Table 4. They are of the order 3.5 eV and vary by only 0.02 eV among the cluster isomers 8A, 8B, and 8G within the same level of theory. Consequently, the relative energies of the clusters hardly shift and the energetic ordering is preserved by including the vibrational zero-point correction.

The vibration frequencies of the clusters 8A, 8B, and 8G are shown in units of wavenumbers ( $\text{cm}^{-1}$ ) in Table 7 in the Appendix. For clusters 8A and 8B, the three

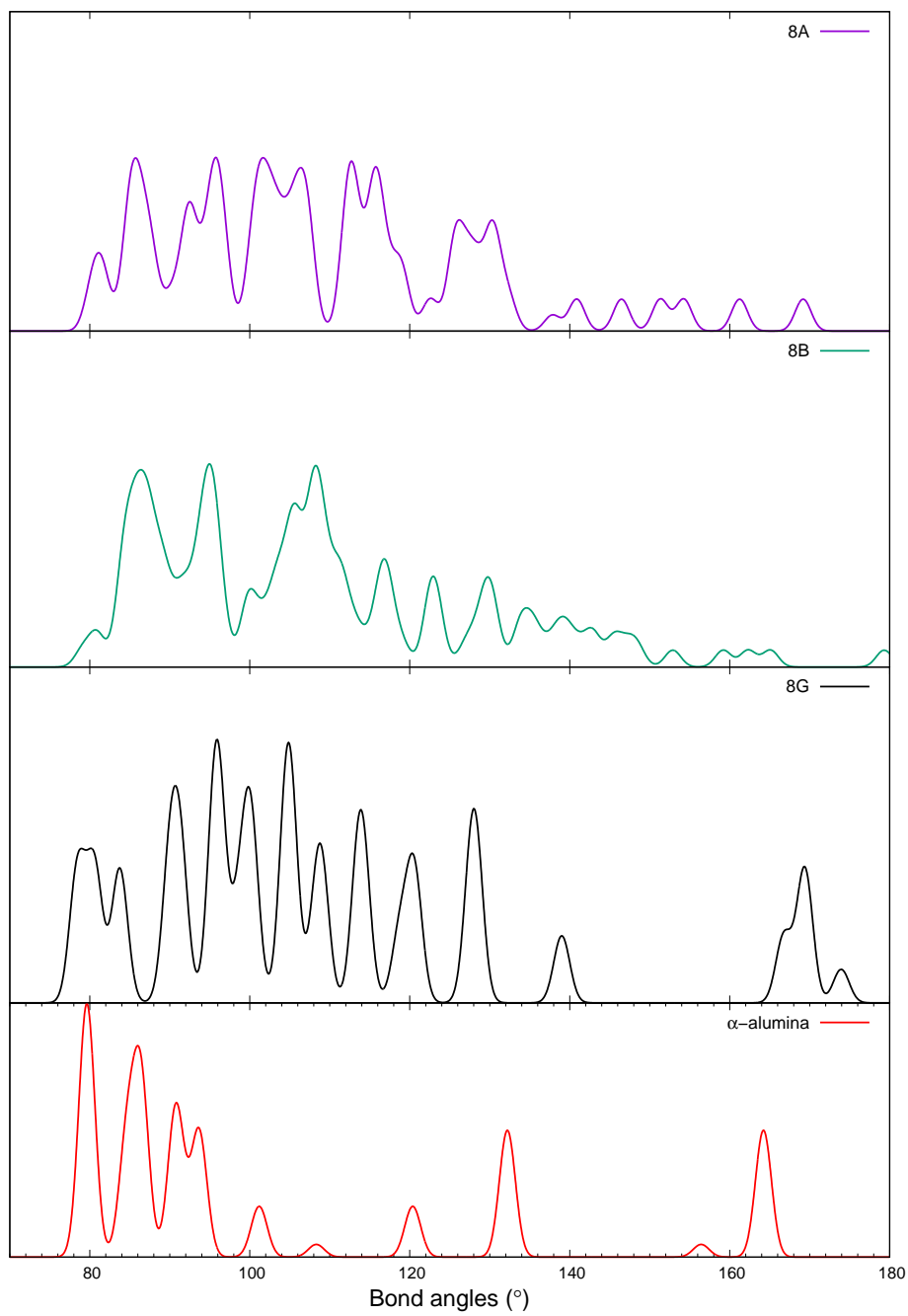


Figure 8: The Al-O-Al and O-Al-O bond angles of structures 8A 8B, 8G and alpha-alumina. The curves are fitted with a Gaussian distribution and a half width  $\gamma=1.0^\circ$  .

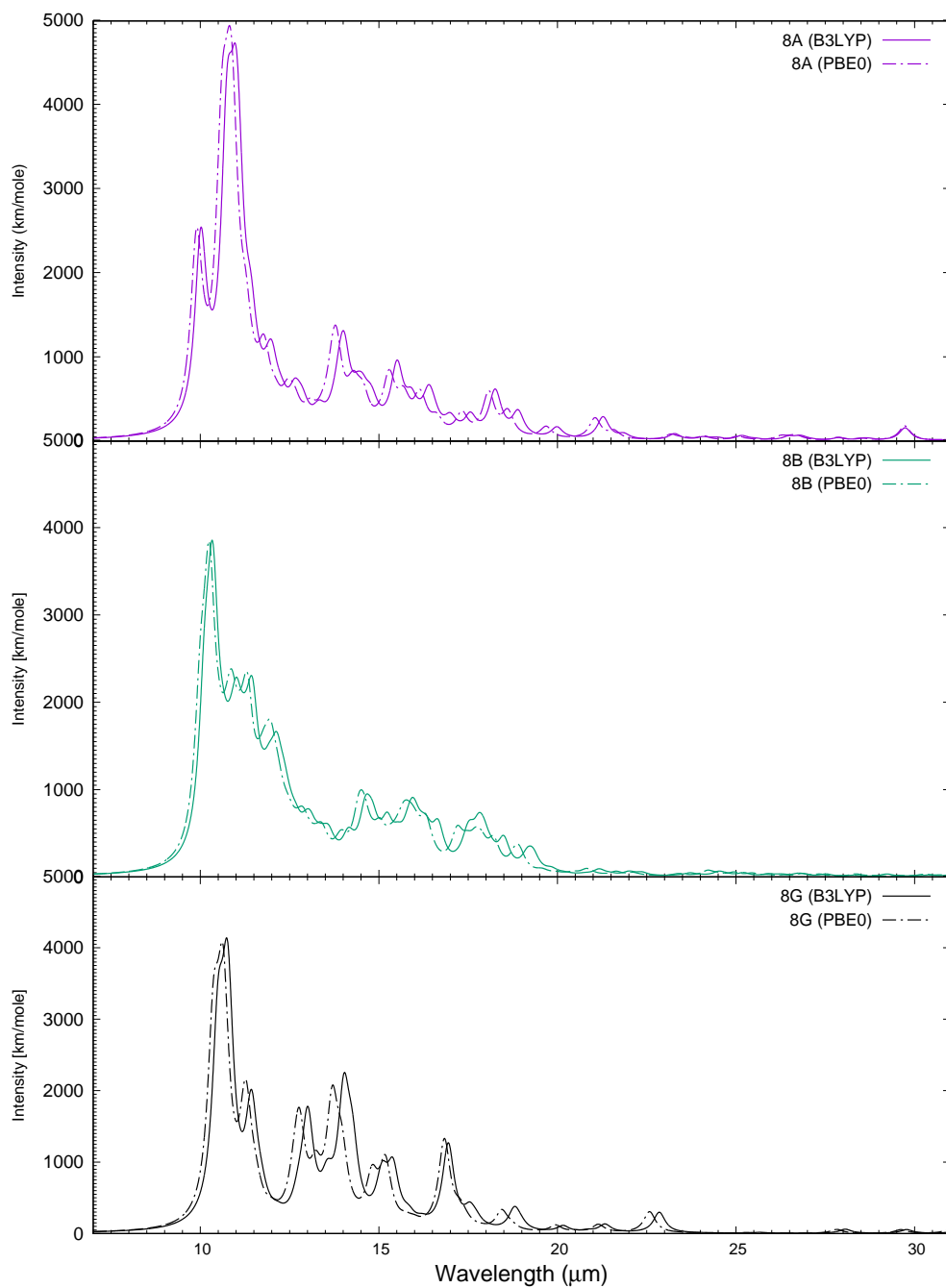


Figure 9: The vibration modes and related intensities of the newly-discovered clusters 8A, 8B, and 8G fitted by a Lorentzian profile with a half width  $\gamma=0.2$ . Straight lines: B3LYP, dashed lines: PBE0.

Table 4: Vibrational zero-point corrections  $\epsilon_0$  (in eV) of 8A, 8B, and 8G as calculated with the B3LYP and the PBE0 functional.

Isomer	$\epsilon_0(\text{B3LYP})$	$\epsilon_0(\text{PBE0})$
8A	3.50	3.54
8B	3.51	3.55
8G	3.49	3.54

lowest modes are located slightly below  $130 \text{ cm}^{-1}$ . In the harmonic oscillator approximation used in the present study, these low frequency modes are associated with hindered rotations rather than vibrations. No imaginary frequency occurs for structures 8A, 8B, and 8G.

### 3.6. Thermochemistry

We calculate thermochemical potentials (heat capacity  $c_P$ , entropy  $S$ , enthalpy of formation  $\Delta H_f(T)$  and the (Gibbs) free energy of formation)  $\Delta G_f(T)$  of both clusters 8A and 8B as a function of temperature (see Tables 5 and 6 in the Appendix). We use a script provided by [31] to calculate the heat capacity  $c_p(T)$ , entropy  $S(T)$  and enthalpy  $H^0(T)$  from the cluster calculation output. In order to determine  $dH_f$  and  $dG_f$ , we follow the approach of Ochterski (see [28]) and make use of the enthalpies and the entropies of the elements (Al and O) in their standard states listed the NIST-JANAF Thermochemical Tables <sup>1</sup>. As the fugacity of elemental gas-phase Al is 1 bar at 2790.81 K we constrain the temperature range to a maximum of  $T = 2700 \text{ K}$ .

The thermodynamic tables for structures 8A and 8B can be found in the Appendix. They are evaluated at a pressure of  $p = 1 \text{ atm}$ . At 0 K the entropy  $dS$  is vanishing by definition and  $dH_f$  equals  $dG_f$ . We derive  $dH_f = -9114.5 \text{ kJ/mole}$  for 8A and  $dH_f = -9100.3 \text{ kJ/mole}$  for 8B – in agreement with the relative potential energies including the zero-point correction. At 298.15 K the situation is similar and the relative enthalpies and Gibbs free energies differ by 13–17  $\text{kJ mole}^{-1}$ . Also for larger temperatures, structure 8A is slightly more favored to form than structure 8B as calculated within the B3LYP density functional. Around  $T = 1400\text{--}1500 \text{ K}$ , the Gibbs free energy of formation for structures 8A and 8B changes sign and becomes positive (endergonic) for larger temperatures. The stability limits of the most stable, smaller-sized ( $n < 8$ ) alumina clusters are similar to those of 8A and 8B, and range from  $T=1300\text{--}1450 \text{ K}$ . We find a slight increase of the critical temperature with cluster size. Thus, an effective alumina octomer formation is expected to occur for temperatures below 1400 K and to be hampered for temperatures larger than 1500 K (at standard pressure of 1 atm). Interestingly, the latter temperature coincides with the condensation temperature for alumina grains in circumstellar conditions[32].

---

<sup>1</sup><https://janaf.nist.gov/>

## 4. Conclusion

We report the discovery of six  $(\text{Al}_2\text{O}_3)_8$  isomers (8A, 8B, 8C, 8D, 8E, 8F) that represent currently the lowest-energy alumina octomer structures known. The octomer is the smallest cluster size at which we find differences with previously reported candidate global minima. All six favourable octomer structures are neither hollow nor spherical, but exhibit elongated and “semi-compact” geometries. The IR spectra of the lowest-energy octomers is dominated by Al-O vibration modes in 10-11  $\mu\text{m}$  wavelength range. By comparing formal charges, bond lengths and angles of the reported low-energy octomers to those of crystalline  $\alpha$ -alumina, we conclude that, at a cluster size  $n=8$ , the alumina bulk limit is not (yet) reached. However, we find that the thermal stability limit of the octomers and smaller-sized polymers in the gas phase coincides with the glass-liquid phase transition of liquid alumina.

*Acknowledgements* This work was supported by the ERC consolidator grant 646758 “AEROSOL”. We acknowledge Dr. Amol D. Rahane for providing the cluster geometries from their studies for comparison. Moreover, we acknowledge the “Accordo Quadro INAF-CINECA (2017)”, for the availability of high performance computing resources and support. This work was supported by a STSM Grant from COST Action CM1401 (“Our AstroChemical History”). This research was supported by the Spanish MINECO/FEDER CTQ2015-64618-R grant and, in part, by Generalitat de Catalunya (grants 2017SGR13 and XRQTC).

## References

### References

- [1] R. P. Turco, R. C. Whitten, O. B. Toon, Stratospheric aerosols: Observation and theory, *Reviews of Geophysics* 20 (2) (1982) 233–279. [arXiv:https://agupubs.onlinelibrary.wiley.com/doi/pdf/10.1029/RG020i002p00233](https://arxiv.org/abs/https://agupubs.onlinelibrary.wiley.com/doi/pdf/10.1029/RG020i002p00233), doi:10.1029/RG020i002p00233.  
URL <https://agupubs.onlinelibrary.wiley.com/doi/abs/10.1029/RG020i002p00233>
- [2] Karovicova, I., Wittkowski, M., Ohnaka, K., Boboltz, D. A., Fossat, E., Scholz, M., New insights into the dust formation of oxygen-rich agb stars, *A&A* 560 (2013) A75. doi:10.1051/0004-6361/201322376.  
URL <https://doi.org/10.1051/0004-6361/201322376>
- [3] Gobrecht, D., Cherchneff, I., Sarangi, A., Plane, J. M. C., Bromley, S. T., Dust formation in the oxygen-rich agb star *ik tauri*, *A&A* 585 (2016) A6. doi:10.1051/0004-6361/201425363.  
URL <https://doi.org/10.1051/0004-6361/201425363>
- [4] Decin, L., Richards, A. M. S., Waters, L. B. F. M., Danilovich, T., Gobrecht, D., Khouri, T., Homan, W., Bakker, J. M., Van de Sande, M., Nuth, J. A., De Beck, E., Study of the aluminium content in agb winds using *alma* - indications for the presence of gas-phase  $(\text{al}_2\text{o}_3)_n$  clusters, *A&A* 608 (2017) A55. doi:10.1051/0004-6361/201730782.  
URL <https://doi.org/10.1051/0004-6361/201730782>
- [5] A. Takigawa, T. Kamizuka, S. Tachibana, I. Yamamura, Dust formation and wind acceleration around the aluminum oxide-rich agb star *w hydrae*, *Science Advances* 3 (11). [arXiv:http://advances.sciencemag.org/content/3/11/eaao2149.full.pdf](https://arxiv.org/abs/http://advances.sciencemag.org/content/3/11/eaao2149.full.pdf), doi:10.1126/sciadv.aao2149.  
URL <http://advances.sciencemag.org/content/3/11/eaao2149>
- [6] S. T. Bromley, J. C. Gomez Martin, J. M. C. Plane, Under what conditions does  $(\text{si}_2\text{o})_n$  nucleation occur? a bottom-up kinetic modelling evaluation, *Phys. Chem. Chem. Phys.* 18 (2016) 26913–26922. doi:10.1039/C6CP03629E.  
URL <http://dx.doi.org/10.1039/C6CP03629E>
- [7] H.-P. Gail, M. Scholz, A. Pucci, Silicate condensation in *Mira* variables, *aap* 591 (2016) A17. [arXiv:1604.04636](https://arxiv.org/abs/1604.04636), doi:10.1051/0004-6361/201628113.

- [8] J. S. Bhatt, I. J. Ford, Investigation of mgo as a candidate for the primary nucleating dust species around m stars, *Monthly Notices of the Royal Astronomical Society* 382 (1) (2007) 291–298. [arXiv:/oup/backfile/content\\_public/journal/mnras/382/1/10.1111/j.1365-2966.2007.12358.x/2/mnras0382-0291.pdf](https://arxiv.org/abs/2007.12358), doi:10.1111/j.1365-2966.2007.12358.x.  
URL <http://dx.doi.org/10.1111/j.1365-2966.2007.12358.x>
- [9] T. M. Koehler, H.-P. Gail, E. Sedlmayr, MgO dust nucleation in M-Stars: calculation of cluster properties and nucleation rates., *aap* 320 (1997) 553–567.
- [10] L. R. Nittler, C. M. O. Alexander, R. Gallino, P. Hoppe, A. N. Nguyen, F. J. Stadermann, E. K. Zinner, Aluminum-, Calcium- and Titanium-rich Oxide Stardust in Ordinary Chondrite Meteorites, *apj* 682 (2008) 1450–1478. [arXiv:0804.2866](https://arxiv.org/abs/0804.2866), doi:10.1086/589430.
- [11] F. Gyngard, E. Zinner, L. R. Nittler, A. Morgand, F. J. Stadermann, K. Mairin Hynes, Automated NanoSIMS Measurements of Spinel Stardust from the Murray Meteorite, *apj* 717 (2010) 107–120. [arXiv:1006.4355](https://arxiv.org/abs/1006.4355), doi:10.1088/0004-637X/717/1/107.
- [12] L. D. Hart, Alumina chemicals, Columbus, OH (USA); American Ceramic Society Inc., United States, 1990.  
URL <http://www.osti.gov/scitech/servlets/purl/5158074>
- [13] M. R. Noordn, K. Y. Liew, Synthesis of Alumina Nanofibers and Composites, InTech, Rijeka, 2010. doi:10.5772/8165.  
URL <http://dx.doi.org/10.5772/8165>
- [14] J.-H. Kim, S.-J. Yoo, D.-H. Kwak, H.-J. Jung, T.-Y. Kim, K.-H. Park, J.-W. Lee, Characterization and application of electrospun alumina nanofibers, *Nanoscale Research Letters* 9 (1) (2014) 44. doi:10.1186/1556-276X-9-44.  
URL <https://doi.org/10.1186/1556-276X-9-44>
- [15] V. Piriawong, V. Thongpool, P. Asanithi, P. Limsuwan, Preparation and characterization of alumina nanoparticles in deionized water using laser ablation technique, *J. Nanomaterials* 2012 (2012) 2:2-2:2. doi:10.1155/2012/819403.  
URL <http://dx.doi.org/10.1155/2012/819403>
- [16] I. P. Batra, Electronic structure of -al 2 o 3, *Journal of Physics C: Solid State Physics* 15 (26) (1982) 5399.  
URL <http://stacks.iop.org/0022-3719/15/i=26/a=019>
- [17] D. van Heijnsbergen, K. Demyk, M. A. Duncan, G. Meijer, G. von Helden, Structure determination of gas phase aluminum oxide clusters, *Phys. Chem. Chem. Phys.* 5 (2003) 2515–2519. doi:10.1039/B212654K.  
URL <http://dx.doi.org/10.1039/B212654K>
- [18] M. Sierka, J. Dbler, J. Sauer, G. Santambrogio, M. Brmmer, L. Wste, E. Janssens, G. Meijer, K. Asmis, Unexpected structures of aluminum oxide clusters in the gas phase, *Angewandte Chemie International Edition* 46 (18) (2007) 3372–3375. [arXiv:https://onlinelibrary.wiley.com/doi/pdf/10.1002/anie.200604823](https://arxiv.org/abs/https://onlinelibrary.wiley.com/doi/pdf/10.1002/anie.200604823), doi:10.1002/anie.200604823.  
URL <https://onlinelibrary.wiley.com/doi/abs/10.1002/anie.200604823>
- [19] A. B. Rahane, M. D. Deshpande, V. Kumar, Structural and electronic properties of (al2o3)n clusters with n = 110 from first principles calculations. *The Journal of Physical Chemistry C* 115 (37) (2011) 18111–18121. [arXiv:https://doi.org/10.1021/jp2050614](https://arxiv.org/abs/https://doi.org/10.1021/jp2050614), doi:10.1021/jp2050614.  
URL <https://doi.org/10.1021/jp2050614>
- [20] R. Li, L. Cheng, Structural determination of (al2o3)n (n=17) clusters based on density functional calculation, *Computational and Theoretical Chemistry* 996 (2012) 125 – 131. doi:<https://doi.org/10.1016/j.comptc.2012.07.027>.  
URL <http://www.sciencedirect.com/science/article/pii/S2210271X12003726>
- [21] Q. Zhang, L. Cheng, Structural determination of (al2o3)n (n = 115) clusters based on graphic processing unit, *Journal of Chemical Information and Modeling* 55 (5) (2015) 1012–1020, pMID: 25928795. [arXiv:https://doi.org/10.1021/acs.jcim.5b00069](https://arxiv.org/abs/https://doi.org/10.1021/acs.jcim.5b00069), doi:10.1021/acs.jcim.5b00069.  
URL <https://doi.org/10.1021/acs.jcim.5b00069>
- [22] D. Wales, J. Doye, Global Optimization by Basin-Hopping and the Lowest Energy Structures of Lennard-Jones Clusters Containing up to 110 Atoms, eprint [arXiv:cond-mat/9803344](https://arxiv.org/abs/cond-mat/9803344)[arXiv:cond-mat/9803344](https://arxiv.org/abs/cond-mat/9803344).
- [23] S. T. Bromley, E. Flikkema, Columnar-to-disk structural transition in nanoscale (sio2)<sub>N</sub> clusters, *Phys. Rev. Lett.* 95 (2005) 185505. doi:10.1103/PhysRevLett.95.185505.  
URL <https://link.aps.org/doi/10.1103/PhysRevLett.95.185505>
- [24] S. M. Woodley, P. D. Battle, J. D. Gale, C. Richard A. Catlow, The prediction of inorganic crystal structures using a genetic algorithm and energy minimisation, *Phys. Chem. Chem. Phys.* 1 (1999)

- 2535–2542. doi:10.1039/A901227C.  
 URL <http://dx.doi.org/10.1039/A901227C>
- [25] T. S. Bush, J. D. Gale, C. R. A. Catlow, P. D. Battle, Self-consistent interatomic potentials for the simulation of binary and ternary oxides, *J. Mater. Chem.* 4 (1994) 831–837. doi:10.1039/JM9940400831.  
 URL <http://dx.doi.org/10.1039/JM9940400831>
- [26] A. D. Becke, A new mixing of Hartree-Fock and local density-functional theories, *jcp* 98 (1993) 1372–1377. doi:10.1063/1.464304.
- [27] J. P. Perdew, M. Ernzerhof, K. Burke, Rationale for mixing exact exchange with density functional approximations, *jcp* 105 (1996) 9982–9985. doi:10.1063/1.472933.
- [28] M. J. Frisch, G. W. Trucks, H. B. Schlegel, G. E. Scuseria, M. A. Robb, J. R. Cheeseman, G. Scalmani, V. Barone, B. Mennucci, G. A. Petersson, H. Nakatsuji, M. Caricato, X. Li, H. P. Hratchian, A. F. Izmaylov, J. Bloino, G. Zheng, J. L. Sonnenberg, M. Hada, M. Ehara, K. Toyota, R. Fukuda, J. Hasegawa, M. Ishida, T. Nakajima, Y. Honda, O. Kitao, H. Nakai, T. Vreven, J. A. Montgomery, Jr., J. E. Peralta, F. Ogliaro, M. Bearpark, J. J. Heyd, E. Brothers, K. N. Kudin, V. N. Staroverov, R. Kobayashi, J. Normand, K. Raghavachari, A. Rendell, J. C. Burant, S. S. Iyengar, J. Tomasi, M. Cossi, N. Rega, J. M. Millam, M. Klene, J. E. Knox, J. B. Cross, V. Bakken, C. Adamo, J. Jaramillo, R. Gomperts, R. E. Stratmann, O. Yazyev, A. J. Austin, R. Cammi, C. Pomelli, J. W. Ochterski, R. L. Martin, K. Morokuma, V. G. Zakrzewski, G. A. Voth, P. Salvador, J. J. Dannenberg, S. Dapprich, A. D. Daniels, . Farkas, J. B. Foresman, J. V. Ortiz, J. Cioslowski, D. J. Fox, Gaussian09 Revision E.01, gaussian Inc. Wallingford CT 2009.
- [29] Y. Gu, N. Xu, M. Lin, K. Tan, Structures, stabilities and properties of hollow (al<sub>2</sub>o<sub>3</sub>)<sub>n</sub> clusters (n=10, 12, 16, 18, 24 and 33): Studied with density functional theory, *Computational and Theoretical Chemistry* 1063 (2015) 29 – 34. doi:<https://doi.org/10.1016/j.comptc.2015.03.027>.  
 URL <http://www.sciencedirect.com/science/article/pii/S2210271X15001425>
- [30] H. P. Pinto, R. M. Nieminen, S. D. Elliott, Ab initio study of  $\gamma$ -al<sub>2</sub>o<sub>3</sub> surfaces, *Physical Review B* 70 (12). doi:10.1103/physrevb.70.125402.  
 URL <https://doi.org/10.1103/physrevb.70.125402>
- [31] K. K. Irikura, D. J. Frurip, *Computational Thermochemistry*, American Chemical Society, Washington, DC, 1998. arXiv:<https://pubs.acs.org/doi/pdf/10.1021/bk-1998-0677>, doi:10.1021/bk-1998-0677.  
 URL <https://pubs.acs.org/doi/abs/10.1021/bk-1998-0677>
- [32] F. J. Molster, L. B. F. M. Waters, F. Kemper, The Mineralogy of Interstellar and Circumstellar Dust in Galaxies, in: T. Henning (Ed.), *Lecture Notes in Physics*, Berlin Springer Verlag, Vol. 815 of *Lecture Notes in Physics*, Berlin Springer Verlag, 2010, pp. 143–201. doi:10.1007/978-3-642-13259-9\_3.

## 5. Appendix

Table 7: Vibration frequencies (in cm<sup>-1</sup>) of structures 8A, 8B, and 8G, respectively, as calculated on the B3LYP/6-311+G(d) level of theory.

8A					
90.2094	103.6610	113.1299	113.7897	126.2836	132.1154
149.5395	156.1298	158.4286	161.9488	174.7097	178.0820
184.1340	190.3925	204.5866	208.6846	221.3737	224.7862
234.3400	239.6439	242.4419	247.5123	258.1091	263.3042
270.1901	274.4194	278.7248	281.9794	282.3983	287.7413
288.8951	296.8160	298.2015	304.0709	313.6256	317.7489
319.7042	323.7852	336.3023	341.3491	348.0401	349.9338
358.6037	368.5844	372.0300	373.5352	377.7690	385.1710
391.3964	396.4796	397.9887	408.3760	411.1994	415.4799
429.5667	445.8082	454.5025	457.4732	468.7610	470.0209

500.3456	528.1360	529.2779	531.0116	543.8943	546.9150
548.7668	567.2123	569.4951	579.9749	588.3215	596.2581
604.8862	610.0111	619.6286	621.5216	628.7537	642.1270
644.2739	646.3816	657.8524	673.2383	677.6540	687.9148
695.1378	700.3167	712.7577	718.9825	728.6398	744.8394
750.7953	776.8708	778.8075	785.2246	789.7197	791.7034
814.7539	819.7563	830.9581	833.2751	841.4871	849.4601
858.8782	873.2397	876.3019	884.4792	902.1171	903.8100
910.3530	912.0732	927.6888	932.0930	977.5391	998.7102
8B					
91.5358	102.2772	127.9649	131.8299	138.9168	148.8552
162.9458	164.5536	170.5986	182.0207	182.4413	191.8727
195.4770	201.6917	209.1333	214.7327	219.3009	226.7387
237.6343	244.6223	257.7512	260.7836	263.6712	269.5421
272.3050	275.5059	276.6740	281.4691	284.9971	290.0597
300.2656	305.9572	310.1684	314.8178	321.0454	323.5269
328.9138	334.0525	335.7036	341.8931	343.0069	353.5171
363.3137	371.8111	374.0156	380.3567	381.6630	386.0263
396.6048	404.7217	407.9325	416.3372	421.6654	427.1868
438.9616	447.2230	454.3461	465.7418	472.3817	481.2743
495.0933	504.2488	517.5900	521.9706	540.6087	550.9677
557.2089	561.7813	570.0408	573.0887	580.7838	596.3860
600.3627	611.0725	613.8789	617.0713	623.8788	627.7754
633.1866	644.1204	656.4854	665.7699	674.8369	683.6253
689.7383	701.3332	706.8205	712.2638	724.6251	735.9241
744.9986	750.8257	763.5632	768.4292	773.4613	788.8824
799.3710	809.5934	813.1208	822.8043	824.5475	837.2392
841.2173	851.2534	871.5892	873.8353	883.6798	893.3444
908.3880	922.3289	938.0098	942.0166	966.3894	987.5792
8G					
122.3280	122.3759	129.8718	131.3459	135.3512	135.3567
160.7597	160.7656	183.8549	186.7616	187.1831	204.2287
204.2723	217.8290	220.2045	229.5106	229.5346	231.3625
231.8471	239.0043	239.1124	252.2576	269.6685	272.3767
281.5665	282.3724	282.3769	282.9120	286.2491	291.0896
291.1085	302.0007	318.3927	321.6422	321.6754	335.8252
335.8279	340.0566	346.0378	356.3743	356.3883	357.4173
382.5699	387.4643	389.4900	395.7846	395.7900	428.6817
429.0807	437.5835	437.6173	465.4728	468.8242	468.8270
479.5008	479.5210	496.0409	499.3839	511.9482	520.9266
527.3433	527.8370	532.0045	532.0267	552.8827	557.4152
558.3805	559.2673	563.9438	563.9612	569.7835	569.8415
590.0452	590.1963	590.2086	615.5018	616.9330	616.9430
631.5871	634.1916	640.4553	640.4813	643.1729	649.5379
662.7197	662.7357	664.9720	669.2429	701.3175	701.3529
713.2892	726.5958	728.8081	737.7250	737.7345	757.0507

768.7273	768.7298	783.9297	788.5174	816.6344	822.2092
822.2348	850.9110	853.7232	853.8241	857.5930	865.4159
874.7006	874.7399	898.7439	928.8732	928.9094	952.6200

Table 5: Thermodynamic quantities (temperature T, entropy S, heat capacity  $c_P$ , enthalpy change  $H(T)-H(0)$ , enthalpy of formation  $dH_f$  and Gibbs free energy of formation  $dG_f$  of 8A. Units are K for T,  $\text{JK}^{-1}\text{mol}^{-1}$  for S and  $c_P$ , and  $\text{kJmol}^{-1}$  for  $H(T)-H(0)$ ,  $dH_f$  and  $dG_f$ .

T	S	$C_P$	$H(T)-H(0)$	$dH_f$ (kJ/m)	$dG_f$
0.00	0.000	0.000	0.000	-9114.469	-9114.469
100.00	395.149	205.289	9.052	-9055.689	-8545.540
200.00	619.018	459.222	42.819	-8992.442	-7887.085
250.00	732.484	558.040	68.335	-8957.766	-7554.811
298.15	837.577	634.649	97.118	-8922.095	-7234.368
300.00	841.510	637.258	98.295	-8920.662	-7222.025
350.00	944.617	699.536	131.778	-8881.499	-6889.260
400.00	1041.339	748.222	168.022	-8840.751	-6556.870
450.00	1131.760	786.395	206.426	-8798.843	-6225.041
500.00	1216.237	816.552	246.528	-8756.149	-5893.967
600.00	1369.237	860.003	330.512	-8669.469	-5234.332
700.00	1504.114	888.813	418.046	-8582.487	-4578.544
800.00	1624.174	908.693	507.979	-8496.474	-3927.026
900.00	1732.067	922.903	599.597	-8412.296	-3280.074
1000.00	1829.874	933.372	692.436	-8500.065	-2807.347
1100.00	1919.221	941.289	786.186	-8415.723	-2164.472
1200.00	2001.398	947.410	880.634	-8331.227	-1523.173
1300.00	2077.429	952.234	975.625	-8246.644	-883.305
1400.00	2148.144	956.101	1071.049	-8162.028	-244.770
1500.00	2214.219	959.246	1166.822	-8077.399	392.473
1600.00	2276.212	961.836	1262.880	-7992.845	1028.525
1700.00	2334.590	963.995	1359.174	-7908.359	1663.434
1800.00	2389.743	965.812	1455.667	-7823.970	2297.288
1900.00	2442.004	967.356	1552.328	-7739.733	2930.067
2000.00	2491.658	968.678	1649.131	-7655.602	3561.866
2100.00	2538.948	969.819	1746.057	-7571.660	4192.683
2200.00	2584.087	970.810	1843.090	-7487.851	4822.595
2300.00	2627.261	971.677	1940.215	-7404.230	5451.636
2400.00	2668.632	972.439	2037.422	-7320.775	6079.827
2500.00	2708.343	973.113	2134.700	-7237.505	6707.158
2600.00	2746.521	973.711	2232.042	-7154.387	7333.788
2700.00	2783.279	974.245	2329.440	-7071.437	7959.704

Table 6: Thermodynamic quantities (temperature T, entropy S, heat capacity  $c_P$ , enthalpy change  $H(T)-H(0)$ , enthalpy of formation  $dH_f$  and Gibbs free energy of formation  $dG_f$  of isomer 8B. Units are K for T,  $\text{JK}^{-1}\text{mol}^{-1}$  for S and  $c_P$ , and  $\text{kJmol}^{-1}$  for  $H(T)-H(0)$ ,  $dH_f$  and  $dG_f$ .

T	$c_P$	$H(T)-H(0)$	$dH_f$	$dG_f$
0.00	0.000	0.000	-9100.292	-9100.292
100.00	387.576	197.744	-9041.969	-8531.063
200.00	607.633	456.565	-8979.243	-7871.609
250.00	720.715	557.171	-8944.651	-7538.753
298.15	825.748	634.774	-8908.995	-7217.741
300.00	829.682	637.411	-8907.563	-7205.378
350.00	932.857	700.208	-8868.377	-6872.022
400.00	1029.685	749.124	-8827.589	-6539.047
450.00	1120.218	787.372	-8785.634	-6206.638
500.00	1204.798	817.523	-8742.890	-5874.989
600.00	1357.967	860.870	-8656.119	-5214.220
700.00	1492.968	889.549	-8569.056	-4557.311
800.00	1613.118	909.310	-8482.975	-3904.682
900.00	1721.078	923.422	-8398.741	-3256.628
1000.00	1818.935	933.812	-8486.462	-2782.805
1100.00	1908.322	941.664	-8402.079	-2138.839
1200.00	1990.528	947.733	-8317.549	-1496.451
1300.00	2066.583	952.515	-8232.935	-855.496
1400.00	2137.318	956.347	-8148.293	-215.879
1500.00	2203.409	959.462	-8063.642	422.445
1600.00	2265.415	962.028	-7979.067	1059.578
1700.00	2323.804	964.166	-7894.562	1695.567
1800.00	2378.967	965.966	-7810.157	2330.498
1900.00	2431.236	967.495	-7725.906	2964.353
2000.00	2480.896	968.804	-7641.761	3597.231
2100.00	2528.192	969.934	-7557.807	4229.124
2200.00	2573.337	970.915	-7473.988	4860.108
2300.00	2616.515	971.774	-7390.356	5490.226
2400.00	2657.889	972.528	-7306.892	6119.493
2500.00	2697.604	973.195	-7223.613	6747.897
2600.00	2735.785	973.787	-7140.488	7375.601
2700.00	2772.546	974.315	-7057.530	8002.590